Article

High Speed Single Cell Dielectric Spectroscopy

Daniel Spencer, and Hywel Morgan

ACS Sens., **Just Accepted Manuscript** • DOI: 10.1021/acssensors.9b02119 • Publication Date (Web): 04 Feb 2020

High Speed Single Cell Dielectric Spectroscopy

Daniel Spencer and Hywel Morgan*

Electronics and Computer Science, and Institute of Life Sciences University of Southampton, SO17 1BJ, UK.

*Corresponding Author: hm@ecs.soton.ac.uk.

Abstract

Single cell impedance cytometry is a label free analysis technique that is now widely used to measure the electrical properties of cell, and to differentiate different sub-populations. Current techniques are limited to measuring the impedance of a single cell at one or two simultaneous frequencies. Also there are no methods that extrapolate the intrinsic electrical properties of single cells. We demonstrate a new approach that uses multi-frequency impedance measurements to determine the complete intrinsic electrical properties of thousands of single cells at high throughput. The applicability of the method is demonstrated by measuring the properties of red blood cells and red cell ghosts, deriving the unique values of conductivity and permittivity of the membrane and cytoplasm for each individual cell.

Keywords: Single cell analysis, microfluidics, dielectric spectroscopy, cytometry, impedance analysis.

Single cell assay technologies are widely used in microfluidic systems. Single cell analysis enables identification of rare events and observation of the widespread heterogeneity that appears in biological populations. Label-free particle analysis methods are of particular interest since they reflect cell phenotype, such as intrinsic electrical, optical or mechanical properties. One widely used label-free technique is impedance spectroscopy that measures the electrical characteristics of cells. Traditionally, alternating current (AC) electrokinetic methods are used, specifically electrorotation (ROT) and/or dielectrophoresis (DEP) [1-2]. AC electrokinetic methods provide comprehensive data on the electrical parameters of cells but they are not high throughput, although recent techniques have improved this [3-8].

To address these drawbacks, the technique of single cell impedance cytometry was developed, which has become widely used for measuring the impedance of single cells [9-11] It is high throughput and can analyse and differentiate many different sub-populations including human blood, leukaemic cells, pathogens and as. Although high throughput, impedance cytometry has not been able to provide the same level of detail as other AC electrokinetic techniques, i.e. the complete electrical properties of single cells at high throughput.

In this paper we describe a new high speed single cell characterisation method that delivers the full frequency-dependent properties of cells at rates of up to a thousand cells per second. The electrical impedance is measured using 8 simultaneous frequencies. Inherent system non-linearities are removed using normalisation algorithms and the electrical impedance data is analysed using Maxwell's mixture equation with the shell model to extract the unique dielectric parameter set for

each cell. The utility of the technique was demonstrated by measuring the properties of thousands of individual (spherical) red blood cells (RBCs) and ghosts (no haemoglobin in the cytoplasm).

Theory

Single Cell Electrical Model

The electrical properties of a single cell can be represented using an equivalent circuit [12-13] as outlined in Figure 1a. In the simplest analytical model, the cell membrane is represented as a capacitor, which is in series with a resistor-capacitor combination that describes the cytoplasm. In general the cell membrane resistance is extremely high and is ignored (as in the figure). Also the reactance of the cell cytoplasm is much higher than the cytoplasm resistance and is also ignored. The equivalent impedance for the cell is in parallel with two further elements representing the suspending medium. Actual values for these elements depends on cell properties together with the volume fraction of the cell within the measurement system [9, 13]. Because the cell membrane has a very high electrical resistance, at low AC frequencies (<1MHz) cells behave as insulating particles. Low frequency impedance measurements therefore provide a direct measurement of (electrical) cell volume. The cell lipid membrane is only a few nm thick, which translates into a high specific membrane capacitance; typically of the order of 10mF/m^2. At intermediate frequencies, (1-5 MHz) this membrane capacitance dominates the measured impedance spectrum. However, at higher frequencies (>20MHz), the electric field capacitively couples across the membrane and the electrical properties are dominated by the cell cytoplasm conductivity (the cytoplasm permittivity can be ignored) and finally the nucleus (if present) at very high frequencies. Figure 1(b) and (c) illustrates how the impedance spectrum in these three frequency windows changes following small perturbations in cell electrical properties (shaded).

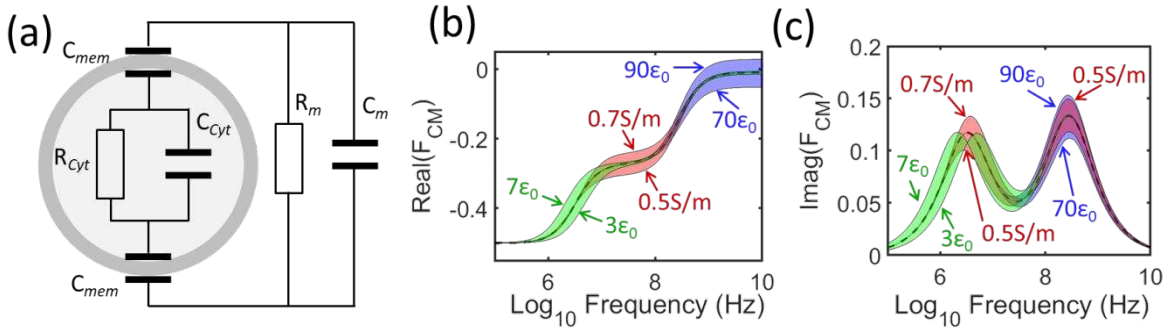

Figure 1. (a) Equivalent circuit model of a simple cell without nucleus suspended in an electrolyte. R_{Cyt} and C_{Cyt} are two circuit elements representing the inner part of the cell. R_m and C_m are the resistance and capacitance of the suspending medium (usually PBS). The cytoplasm capacitance is in series with the C_{mem}, the cell membrane capacitance (membrane resistance is generally ignored). Fig 1 (b) and (c) show calculated examples of the Real and Imaginary parts of the impedance of a spherical red blood cell (radius=2.75µm, cytoplasm conductivity = 0.6 S/m, membrane permittivity = $4.5\varepsilon_0$, cytoplasm permittivity = $80\varepsilon_0$) suspended in PBS (conductivity = 1.6 S/m). The shaded regions correspond to three frequency windows where differences in the cell electrical properties can be measured, corresponding to: membrane capacitance (green, 3-$7\varepsilon_0$), cytoplasm conductivity (blue, 0.5-0.7 S/m) and cytoplasm permittivity (blue, 70-$90\varepsilon_0$).

The measured impedance spectrum for a cell can be analysed by fitting it to an equivalent circuit (Fig 1a), which then allows approximate values of the individual circuit elements to be determined [9]. Alternatively, the dielectric properties can be determined directly by fitting the spectrum to the so

called shell model [14]. This model approximates the cell to a series of concentric shells, each with a unique conductivity and permittivity. A cell might have one or more shells corresponding to the membrane, cytoplasm, nuclear membrane, nucleoplasm etc; each interface gives rise to a single dielectric dispersion. The cell shown in Fig 1 has a single shell and therefore two dispersions.

The dielectric properties of a mixture of particles can be related to the properties of the individual particles and the suspending solution through Maxwell's mixture theory (MMT). For spherical particles dispersed in a suspending medium with a volume fraction φ, the complex impedance of the mixture is [14]:

$$\tilde{\varepsilon}_{mix} = \tilde{\varepsilon}_m \frac{1+2\varphi\tilde{f}_{CM}}{1-\varphi\tilde{f}_{CM}} = \tilde{\varepsilon}_m \frac{1+2\varphi\left(\frac{\tilde{\varepsilon}_p-\tilde{\varepsilon}_m}{\tilde{\varepsilon}_p+2\tilde{\varepsilon}_m}\right)}{1-\varphi\left(\frac{\tilde{\varepsilon}_p-\tilde{\varepsilon}_m}{\tilde{\varepsilon}_p+2\tilde{\varepsilon}_m}\right)} \quad (1)$$

where $\tilde{\varepsilon}$ is a general complex permittivity, given by $\tilde{\varepsilon} = \varepsilon - j\frac{\sigma}{\omega}$, with ε the permittivity, σ the conductivity, $j^2 = -1$, and ω the angular frequency. Subscripts *p* and *m* refer to particle and medium respectively.

In equation (1) the Clausius Mossotti factor ($\tilde{f}_{CM}$) is defined as:

$$\tilde{f}_{CM} = \frac{\tilde{\varepsilon}_p - \tilde{\varepsilon}_m}{\tilde{\varepsilon}_p + 2\tilde{\varepsilon}_m} \quad (2)$$

For a single shelled particles (i.e. a cell with a membrane), the complex permittivity is given by:

$$\tilde{\varepsilon}_p = \tilde{\varepsilon}_{mem} \frac{\gamma^3 + 2\left(\frac{\tilde{\varepsilon}_i - \tilde{\varepsilon}_{mem}}{\tilde{\varepsilon}_i + 2\tilde{\varepsilon}_{mem}}\right)}{\gamma^3 - \left(\frac{\tilde{\varepsilon}_i - \tilde{\varepsilon}_{mem}}{\tilde{\varepsilon}_i + 2\tilde{\varepsilon}_{mem}}\right)} \quad (3)$$

where $\gamma = R/(R-d)$.

In this equation, *R* is the radius of the cell, *d* the thickness of the cell membrane, and $\tilde{\varepsilon}_i$ and $\tilde{\varepsilon}_{mem}$ the complex permittivities of the interior (cytoplasm) and membrane respectively. This equation can be extended by adding more shells; in general there *n+1* relaxations for *n* shells.

Measurement principle

The microfluidic impedance cytometer consists of a microfluidic channel within which are several micron-sized electrodes, as shown in Fig 2. When an AC voltage is applied to the electrodes, a flowing cell perturbs the electrical current which is measured differentially (one electrode pair followed by a second pair). This signal has an anti-symmetric Gaussian shape, where the peak magnitude corresponds to the cell impedance at that frequency. In microfluidic impedance cytometry, the electrical impedance is generally measured at two frequencies simultaneously; usually a low frequency (e.g. 0.5MHz) to measure cell volume and a higher frequency (1-5MHz) to measure changes

in membrane capacitance (c.f. Fig 1(b) & (c)). Unlike AC electrokinetic techniques, cells are suspended in a high conductivity physiological buffer meaning they are minimally perturbed during the measurement.

In a conventional impedance cytometer a single pair of parallel facing electrode is used, as in Fig 2a. In such a system the electric field between the electrodes is non-uniform meaning that the measured impedance of a particle depends on its vertical position as it flows between the electrodes, i.e. the impedance depends on the trajectory of the particle along the channel [13]. This gives rise to significant errors in the measured impedance for particles that flow off-centre, significantly broadening the coefficient of variation (CV) of the data. Figure 2(b) shows example signals for cells travelling in the centre of the channel (blue) and cells moving along the top (yellow) or bottom (red) of the channel. This error can be significantly reduced by using novel electrode arrangements that introduce additional features into the signals, together with computational analysis of the measured signals [16-17]. Although these methods almost eliminate the positional dependence of the signal, there is a significant computational overhead where large data sets require post-processing by convolution and template fitting. To address this we have developed a simpler system that allows real time analysis of particle data using the improved electrode arrangement shown in Fig 2 (c). The error in the impedance signal due to off-centre particles arises primarily from current leakage to nearest neighbour electrodes as the electric field is distorted in the presence of a particle [15]. In this new design, all non-signal electrode are connected to ground, minimising the leakage current and virtually eliminating off-centre errors [18]. The simulated signals for this electrode arrangement are shown in Fig 2(d), where only minor errors between centre and off-centre particles are seen. This approach provides a hardware rather than software solution, significantly reducing the post-processing overhead.

Fig 2 (e) shows example histograms for a mixture of different sized polystyrene particles measured using both the conventional 2 electrode pair arrangement and the new 5-electrode pair arrangement. The data is the cube root of the low frequency (500kHz) impedance, directly proportional to particle diameter. The figure shows that the 5-electrode arrangement is a significant improvement on the classical 2 electrode pair geometry producing almost Gaussian distributions in particle size. The coefficient of variation (CV) for the beads measured using the 5 electrode system are 3.9, 3.4, 2.8 and 2.0 (for the 3.0, 4.5, 6.0 and 10um diameter beads) which are similar to manufacturer's values (2.8, 3.4, 3.2 and 2.9 respectively).

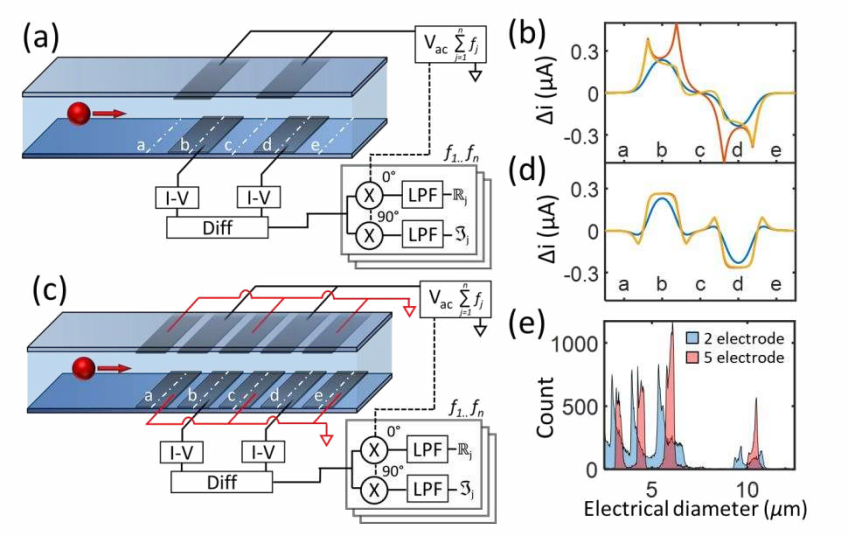

Figure 2. (a) Conventional microfluidic impedance cytometer experimental system using two pairs of electrodes and (b) the differential current signal (determined from a Finite Element simulation – see ESI). Three traces are drawn corresponding to a cell passing through the middle of the channel (blue), close to the top electrodes (yellow) and bottom electrodes (red). (c) new 5 electrode arrangement and (d) corresponding simulated differential current for the same trajectories as in (b). (e) experimental histogram of the electrical diameter (proportional to the cube root of electrical impedance at low frequency (500kHz)) for a mixture of 3, 4.5, 6 and 10 μm diameter particles. The measured CVs from smallest to largest beads are 3.9, 3.4, 2.8 and 2.0% which are similar to the manufacturers reported values of 2.8, 3.9, 3.2 and 3.0%.

System Normalisation

The measured frequency-dependent impedance for a single cell includes effects from the measurement hardware (non-linear behaviour of the electronics and chip parasitics), which need to be compensated. When a cell is placed between two electrodes, the complex impedance of the mixture, $\tilde{Z}_{mix}$, is related to the complex permittivity of the mixture according to the following equation:

$$\tilde{Z}_{mix} = \frac{1}{j\omega\tilde{\varepsilon}_{mix}\kappa} \qquad (4)$$

Here the geometric cell constant κ depends on the dimensions of the measurement volume, including electrode width and spacing. Because the electric field is non-uniform κ cannot be determined precisely, although analytical methods have been developed [19] but these are not applicable to the geometry of Fig 2(c). Furthermore, non-linearities in the measurement electronics and chip, together with the non-linear double layer capacitance means direct measurement of $\tilde{\varepsilon}_{mix}$ is impossible. To address this problem, the system was calibrated by measuring inert particles with well-known dielectric properties. The measured impedance spectrum for these calibration particles provides a unique transfer function for each individual cytometer chip. Polystyrene particles are optimally suited to this, since they have a well-defined size (CV <1%) and electrical properties with typical permittivity, $\varepsilon_p = 2.5\varepsilon_o$. They carry a net surface charge, but their effective conductivity is insignificant compared to the suspending medium (assuming a surface conductance of 1nS, σ_p= 0.3mS/m << σ_m; PBS = 1.6S/m). However, although the beads have fixed permittivity and conductivity their polarizability is not frequency independent and it is important to take this into account during the normalisation. At high frequencies, the beads exhibit a dielectric relaxation, with a characteristic frequency given by:

$$f = \frac{1}{2\pi}\frac{\sigma_p + 2\sigma_m}{\epsilon_p + 2\epsilon_m} \qquad (5)$$

For the particles and suspending medium used in this work, this frequency is 355MHz implying that frequencies greater than 10MHz could be influenced by this relaxation (a classical Debye relaxation is approximately two decades wide in frequency).

Experimentally, the impedance of a cell is determined from the differential current ($\Delta\tilde{i}_{particle}$) as it passes between the measurement electrode pair (see Fig 2). This complex current is related to the impedance of the mixture (particle plus medium) according to the following equation:

$$\Delta\tilde{i}_{particle} = \frac{V\tilde{S}(\omega)}{\tilde{Z}_m} - \frac{V\tilde{S}(\omega)}{\tilde{Z}_{mix}} = j\omega\kappa V\tilde{S}(\omega)\,(\tilde{\varepsilon}_m - \tilde{\varepsilon}_{mix}) \qquad (6)$$

where a complex system transfer function $\tilde{S}(\omega)$ is introduced to account for the non-linear frequency-dependent phase and gain of the measurement system, together with the double layer capacitance (or constant phase element) at the electrode-electrolyte interface. In this equation V is the applied voltage and $\tilde{\varepsilon}_{mix}$ is given by equation (1).

Equation (6) was used to calculate example spectra for model biological cells; a sphered RBC and an RBC ghost, using typical literature parameters for cell properties (see figure legend) and assuming no non-uniformity in the measurement system ($\tilde{S}(\omega) = 1$). The real and imaginary differential currents are plotted in Figure 3 (a) & (b) (blue lines, left hand axis). Both the sphered RBC and ghost show similar spectra for frequencies up to 10MHz. However significant differences between the two cells are seen for higher frequencies due to differences in internal conductivity. The sphered RBCs do not contain haemoglobin and have a conductivity that matches the external medium conductivity. Figure 3 also shows the presence of a second relaxation (more visible in the imaginary part) for the sphered RBCs, which is absent for the ghosts because these have approximately the same internal conductivity as the suspending medium.

Equation 6 was also used to calculate the differential current for a bead ($\Delta\tilde{i}_{bead}$), and values for the ratio of cell to bead current ($\Delta\tilde{i}_{cell}/\Delta\tilde{i}_{bead}$) are plotted in Figure 3 (red lines, right hand axis) for the same sphered RBCs and ghosts. If beads are measured in the same mixture as cells, the transfer function $j\omega\kappa V\tilde{S}(\omega)$ from equation (6) is the same in both cases and the ratio of $\Delta\tilde{i}_{cell}/\Delta\tilde{i}_{bead}$ is independent of the applied voltage, system dimensions or measurement non-linearity:

$$\frac{\Delta\tilde{i}_{cell}}{\Delta\tilde{i}_{bead}} = \frac{j\omega\kappa V\tilde{S}(\omega)(\tilde{\varepsilon}_m - \tilde{\varepsilon}_{mix(cell)})}{j\omega\kappa V\tilde{S}(\omega)(\tilde{\varepsilon}_m - \tilde{\varepsilon}_{mix(bead)})} = \frac{\tilde{\varepsilon}_m - \tilde{\varepsilon}_{mix(cell)}}{\tilde{\varepsilon}_m - \tilde{\varepsilon}_{mix(bead)}} \qquad (7)$$

Figure 3 clearly shows that the dielectric relaxation of the calibration bead has a significant effect on the spectrum, particularly at high frequencies (>10MHz) as seen by the difference between the left and right hand axis. Failure to include this effect would lead to errors in the determined dielectric parameters.

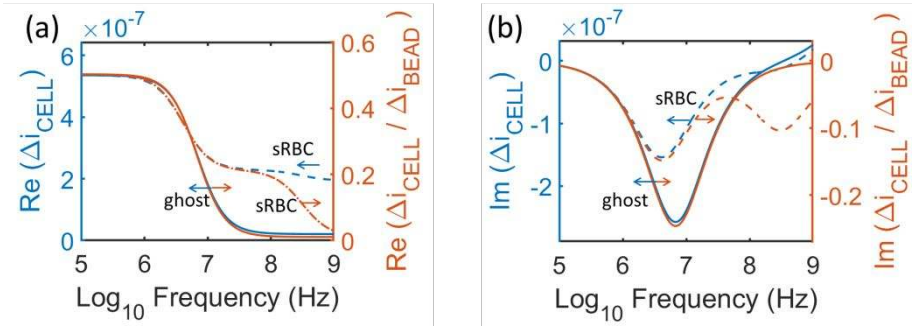

Figure 3. Calculations of the real (a) and imaginary (b) part of the peak differential current for a cell measured between the two electrodes. The left hand axis shows the absolute differential current (blue lines) for ghosts (solid line) and sphered RBCs (dotted line). The right hand axis is the differential current for the cell divided by the differential current for a bead (including the frequency dependent polarizability of the bead) in the same system. The left and right axis are aligned using the real part of the differential current at low frequency. Both spherical RBCs and RBC ghosts were modelled assuming the same volume (90fL), membrane thickness (4.5nm) and permittivity ($4.5\varepsilon_0$), cytoplasm permittivity ($80\varepsilon_0$); with different internal conductivities (ghost σ_i = 1.6 S/m, sRBC σ_i=0.6 S/m). Bead volume =180fL, $\varepsilon_i = 2.5\varepsilon_0$ $\sigma_i = 2K_S/r$ with $K_S = 10^{-9}$S.

Equations (1) and (7) can be combined to give:

$$\frac{\Delta\tilde{i}_{cell}}{\Delta\tilde{i}_{bead}} = \frac{\tilde{f}_{CM(cell)}\varphi_{cell}\ (\tilde{f}_{CM(bead)}\varphi_{bead} - 1)}{\tilde{f}_{CM(bead)}\varphi_{bead}\ (\tilde{f}_{CM(cell)}\varphi_{cell} - 1)} \qquad (8)$$

which for small volume fractions (φ <0.01), simplifies to

$$\Delta\tilde{i}_{cell}/\Delta\tilde{i}_{bead} = \frac{\tilde{f}_{CM(cell)}\,\varphi_{cell}}{\tilde{f}_{CM(bead)}\,\varphi_{bead}} \quad (9)$$

This illustrates that the unknown dielectric properties of the cell ($\tilde{f}_{CM(cell)}$) along with the size (from the volume ratio of the cell to bead ($\frac{\varphi_{cell}}{\varphi_{bead}} = \frac{r_{cell}^3}{r_{bead}^3}$) can be found by multiplying the experimentally measured parameter ($\Delta\tilde{i}_{cell}/\Delta\tilde{i}_{bead}$) by a calibration factor ($\tilde{f}_{CM(bead)}$):

$$\tilde{f}_{CM(cell)}\frac{r_{cell}^3}{r_{bead}^3} = \tilde{f}_{CM(bead)} \times \Delta\tilde{i}_{cell}/\Delta\tilde{i}_{bead} \quad (10)$$

Note that the small volume fraction (φ <0.01) limit means that this method only works for systems with a high signal to noise ratio (SNR) where the channel dimensions are much larger than the cell.

Methods and Materials

Impedance chips

Microfluidic chips were fabricated as described elsewhere [15]. Briefly, metal (Pt) electrodes were lithographically patterned onto glass substrates, with channels 40 µm wide and 30 µm high made from SU8 followed by full wafer bonding. The electrodes are all 30µm wide with 10µm gap. Fluidic and electrical connections were made using custom 3-D printed acrylic interconnects.

Cells were resuspended at a concentration of approximately 500 cells/µL to reduce the probability of doublets in PBS and pumped through the channel with a syringe pump at a flow rate of 40 µL/min. Impedance was measured using a Zurich Instruments impedance scope (HF2IS) and custom PCB front end amplifier board. Either 2 or 8 frequencies were applied simultaneously to the electrodes. A signal of 4 $V_{pk\text{-}pk}$ was used and the differential current sampled at either 56k (8 frequencies) or 230k (2 frequencies) samples per second. Data was processed using custom software written in MATLAB. The impedance of each particle was determined from the peak signal amplitude by convolution for each applied frequency.

RBC processing

RBCs were collected from fingerprick blood from healthy volunteers. In order to simplify analysis and eliminate artefacts due to random orientation of oblate red blood cells, the RBCs were first made spherical following the protocol in [20]. Briefly whole blood was diluted into PBS (10,000:1 v/v) containing 0.3mg/mL Sodium dodecyl sulfate (SDS) and 0.1% glutaraldehyde. SDS is an anionic surfactant that reduces surface tension and at low concentrations spheres the cells. Glutaraldehyde is a common crosslinking agent that has a number of different molecular forms in aqueous solution and reacts with functional groups of proteins including amine, thiol, phenol, and imidazole [21] which cross-links proteins in both the cell membrane and cytoplasm. The sphered RBCs were washed and re-suspended in PBS for measurement. Red cell ghosts were used to measure changes in cytoplasmic properties of cells. These are essentially spherical red cells without haemoglobin with the same electrolyte inside and out. To obtain ghosts, erythrocytes were first lysed in low-ionic concentration Sodium Phosphate (5mM). The membranes were centrifuged and the supernatant discarded. PBS was

then added to the pellet to initiate resealing of the cells. These were fixed by the addition of 0.1% glutaraldehyde (to match the fixed RBCs), washed and resuspended in PBS.

Results

Feature extraction

In order to determine the electrical properties of single cells, the frequency dependent data set for each cell was first fitted using MMT by minimising the mean square error between equation (1) and the experimental data set with the MATLAB function "patternsearch". Pattern search is a direct search function, similar to a brute force method, which searches across a mesh that is defined between the maximum and minimum constraint of each parameter.

The fitting takes the measured impedance signal ($\Delta\tilde{i}_{cell}/\Delta\tilde{i}_{bead}$) and using equation (10) calculates the complex permittivity of the mixture (equation (1)) and the ratio of cell to bead volume fraction, minimising this function. To validate the fitting method, data sets for 1000 different cells were simulated by creating $\tilde{\varepsilon}_{mix(cell)}$ using a random radius, membrane, and cytoplasmic permittivity and conductivity between the search parameter limits at the 8 frequencies used in the single cell experiments (see section 4.3). The values returned by the search function closely matched the values used to create the simulated data set, with a coefficient of variation <0.5%.

Population average data

The RBC is the simplest "model cell" with no nucleus and a membrane with a well-defined capacitance of around 7 to 10mF/m^2. The mean volume of the cell is well maintained at around 80 to 100fL. Figure 4 (a & b) shows a typical impedance spectrum for a population of spherical RBCs and ghosts, after normalisation of the data using 7μm diameter polystyrene beads. The real (Fig 4a) and imaginary (Fig 4b) part of the impedance signal is plotted over a frequency window from 250KHz to 80MHz. This data set was collected using two simultaneous frequencies; one frequency fixed at 18MHz, and a second variable signal that was swept between 250kHz and 80MHz. The 18MHz frequency was used as a reference channel in all frequency sweep experiments as it provides a means to differentiate (and gate) cells from beads. Cells were suspended in PBS and continuously flowed through the cytometer channel whilst the second frequency was swept across the spectrum. Each data point is therefore the average impedance for approximately 1,000 cells. The data shows the distinct Maxwell-Wagner relaxation of the cell membrane, as observed by classical dielectric spectroscopy (9 ,12-13).

The data was normalised following the method outlined in section 2.2 and then fitted to the single shell model (equations 1- 3); the fit is shown by the lines in the figure. Two different fits are shown: the solid line was obtained by setting all dielectric parameters free in the minimisation algorithm, whilst the dotted line (visible at high frequencies in Fig 4(b)) was obtained by fixing the cytoplasmic permittivity to the suspending medium permittivity ($\varepsilon_{Cyt} = 80\varepsilon_o$), i.e. the internal permittivity of the ghosts. In this case a small discrepancy is seen in the imaginary part at high frequencies. From the data set, the mean size and dielectric parameters for the population of spherical red blood cells and ghosts was determined, summarised in Table 1 (all parameters free in the fit). The average membrane capacitance for the sphered RBC was found to be 8.84mF/m^2, with the ghosts slightly lower at 8.55mF/m^2. This is a minor difference and could be because the sphered RBCs were exposed to detergent (SDS) which may have made the membrane slightly thinner. The internal conductivity of

the ghost is 1.4S/m, which is slightly lower than the conductivity of the suspending medium (1.6S/m), probably due to residual low conductivity buffer remaining in the sample after lysing and re-sealing the ghost membranes.

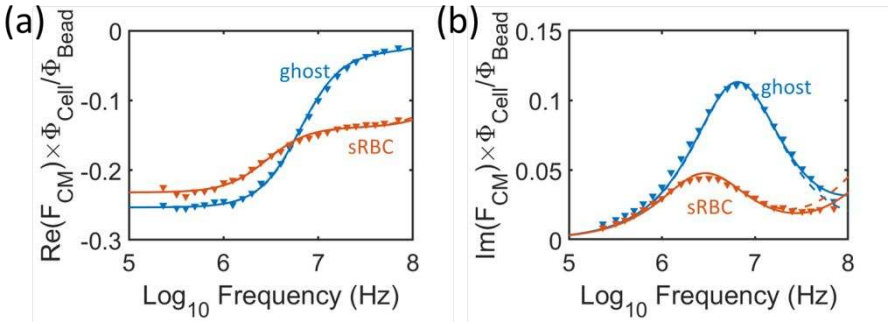

Figure 4. (a-b) Experimentally measured differential current as a function of frequency for a population of sphered red blood cells (red triangles) and ghosts (blue triangles). Polystyrene beads were measured at the same time and used to normalise the system. The y-axis is the real and imaginary components of the Clausius Mossotti factor ($\tilde{f}_{CM}$) multiplied by the ratio of volume fractions for cell to bead. $\tilde{f}_{CM}$ best fit shown as lines. The solid lines are obtained with all parameters free (r, ε_m, ε_i σ_i) while the dotted lines (visible in the imaginary part) are obtained with the permittivity fixed at $80\varepsilon_0$.

Table 1. Summary of fits to the data set in Figure 4. Suspending medium conductivity = 1.6S/m, permittivity = $80\varepsilon_o$.

	Radius (μm)	Volume (fL)	C_{mem}(mF/m²)	ε_{Cyt}	σ_{Cyt}
Sphered RBC	2.7	83	8.89	65	0.52
Ghost	2.8	91	8.40	99	1.40

The dielectric properties of human RBCs has been extensively measured by conventional dielectric spectroscopy and falls within a wide range, between 7mFm^{-2} to as high as^{-2}; see Table 2. These wide variations may reflect the way in which samples were prepared. Comparing Table 1 and 2 shows that our data falls within the range reported by most authors based on measurements using both classical dielectric spectroscopy and single cell electrorotation methods.

Table 2. Summary data for literature values of red blood cell dielectric parameters.

	C_{mem}(mF/m²)	ε_{Cyt}	σ_{Cyt} (S/m)	Technique
[22] Beving 1994	9-10	-	0.458	Dielectric spectroscopy (bulk)
[23] Asami 1988 (mouse)	8.6	52	0.32	Dielectric spectroscopy (bulk)
[24] Gimsa 1996	8.2	212	0.5	Electrorotation
[25] Lisin 1996 (Ghosts)	13.7	-		Impedance spectroscopy
[25] Lisin 1996 (Erythrocyte)	14.3	-		Impedance spectroscopy
[26] Bordi 2002	7-9	-	0.5 – 1.0	
[27] Bao 1994	9	-	0.41	

Single cell spectroscopy

Having demonstrated that microfluidic impedance cytometry can be used to accurately determine the mean dielectric properties of a homogeneous population of cells, we then extended this principle to

measurement of single cells. In this case, rather than use two frequencies, eight frequencies were applied simultaneously to the impedance cytometer electrodes. These frequencies were spaced logarithmically apart between 250kHz and 50MHz. Samples containing sphered red blood cells and ghosts together with reference beads were suspended in PBS and measured as above.

To determine the dielectric properties of individual cells, each single cell spectrum was post-processed by normalising against the mean bead impedance (measured simultaneously) followed by fitting to the shell model using an automated routine in MATLAB. The resulting single cell parameters were then plotted as a set of scatter plots comprising membrane capacitance, cytoplasm conductivity, cytoplasm permittivity and size (electrical radius). These are shown in figures 5 a-c. Each scatter plot consists of 1,000 individual spherical RBCs and 1,000 ghosts.

Examination of Figure 5 shows that the spread in membrane capacitance for the individual sphered RBCs overlaps with the ghosts, consistent with the data for the mean population. Some outlier cells can be identified with an unusually low membrane capacitance. These cells only occur in the ghost population and could be due to double thickness membranes formed during the lysis-resealing process. The data fitting was checked for each of these outliers; Fig S1 shows example spectra of outliers (columns 2-4) where as expected the relaxation frequency is higher in frequency compared to the main population (examples in column 1). For cells suspended in high conductivity suspending media a membrane conductivity of less than 10^{-3}S/m has virtually no influence on the electrical impedance [28]. During the fit, the membrane conductivity is set to zero so that the few outlier cells may have damaged "electrically leaky" membranes with very high conductivity. Finally, Fig 5(d) shows and example spectrum for a single ghost, demonstrating the excellent fit to the single shell model.

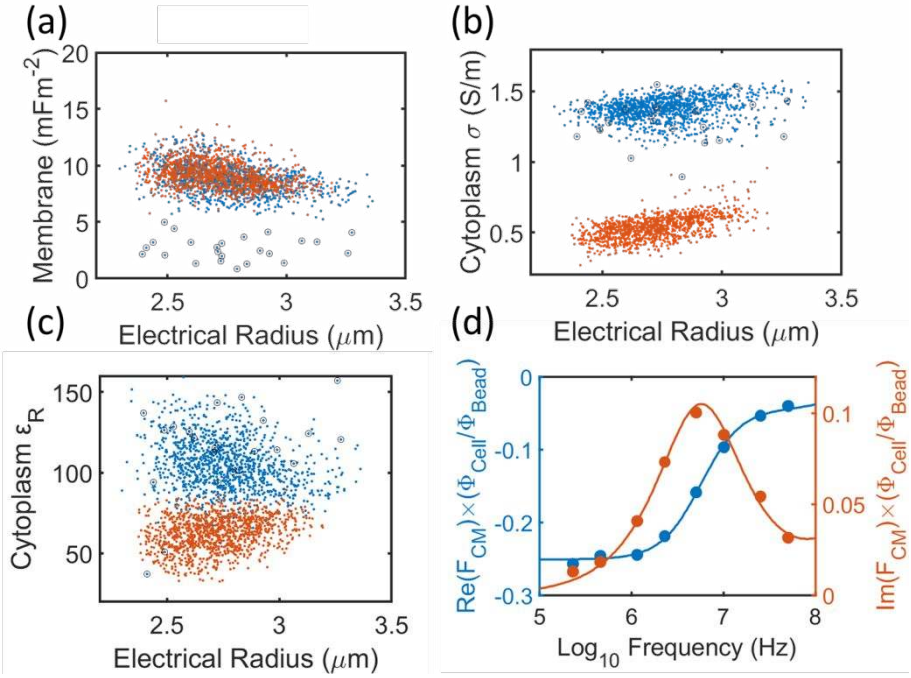

Figure 5. (a-c) Scatter plots showing single cell parameters comprising size (electrical radius) against (a) membrane capacitance, (b) cytoplasm conductivity and (c) cytoplasm permittivity measured for 1,000 individual spherical RBCs and 1,000 ghosts. (d) shows an example electrical impedance spectrum for a ghost cell demonstrating excellent fit to the single shell model.

To confirm the validity of this approach, Figure S2 shows spectra comparing the mean impedance data for each discrete frequency block with the population average data where each frequency is measured

separately (average for all cells in the population). The average of the single cell electrical parameters is shown in table 3, and closely matches the average of the single cell data shown in figure 5(a-c).

Table 3. Summary data for measured red blood cell dielectric parameters, comparing population average data (section 4.2) with the average of the single cell data (section 4.3).

	Electrical radius	Electrical volume (fL)	C_{mem}(mF/m^2)	ε_{Cyt}	σ_{Cyt} (S/m)
Sphered RBC (Average measurement)	2.7	83	8.89	65	0.52
Sphered RBC (Single cell measurements average)	2.7	85	9.19	63	0.53
Ghost (Average measurement)	2.8	91	8.40	99	1.40
Ghost (Single cell measurements average)	2.8	90	8.66	106	1.37

Discussion and conclusions

This work has demonstrated a new approach for high speed single cell characterisation to determine the full frequency-dependent properties of each unique cell. Cells were measured at a throughput of around 400 cells/s (frequency sweep) and 200 cells/s (single cell spectroscopy). The method was tested using spherical RBCs as the simplest "model cell" with no nucleus and well characterised electrical properties. While many biological cells can be approximated to a spherical particle, RBCs are usually a discoid shape. In this work the RBCs were sphered in order to simplify the analysis. Ghost cells were also used since their membranes reseal to a spherical shape and entrap a "cytoplasm" with well-defined dielectric properties.

Glutaraldehyde was used to prepare the iso-volumetrically sphered RBCs, and for consistency the ghost membranes were also fixed with the same concentration of glutaraldehyde. Changes in the electrical properties of single RBCs exposed to different concentrations of glutaraldehyde have been noted by other authors [29-30]. Gagnon *et al* used glutaraldehyde to enhance differences in the electrical properties of aged Bovine RBCs, and reported a decrease in the membrane permittivity from $10.5\varepsilon_0$ to $3.8\varepsilon_0$, along with a decrease in cytoplasm conductivity after fixing with glutaraldehyde [29]. The RBCs were artificially aged in high conductivity saline solution (0.85% NaCl, ~1.2S/m) which is higher than the RBC cytoplasm conductivity and therefore long term storage could have increased cytoplasm conductivity. Furthermore, cells were measured in low conductivity buffer (the zwitterion aminohexanoic acid, 3M) which decreases cytoplasm conductivity by a factor of 10. Cheung *et al* reported an increase in the electrical opacity (>5MHz) of RBCs measured in PBS with increasing glutaraldehyde concentration from 0.002% to 2%, indicating that glutaraldehyde decreases cytoplasm conductivity [30]. This effect could however be due to differences in the shape and orientation of cells in the measurement region because the unfixed cells may deform in the narrow constriction. Bone *et al* reported a small decrease (6%) in the dielectric decrement (membrane capacitance), for a suspension of RBCs after fixing with glutaraldehyde, but at a high concentration of 5% [31]. In this work the same concentration of glutaraldehyde was used to prepare both the RBCs and ghosts so that any effect on the cells would be expected to be minimal and the same for both cell types

This paper has demonstrated and validated a new technique on a well-defined population of cells of spherical geometry. Actual RBC are discoid shapes which can be modelled using an ellipsoidal model [32], however for single cell characterisation the orientation of each cell would need to be known, or alternatively the cell focused into a preferred orientation (for example using dielectrophoresis [33]). Further developments might include multiple sets of electrodes to measure the impedance along several orthogonal directions, but this is beyond the scope of this paper.

The single shell model can be extended to a double shell model for nucleated cells (e.g. white blood cells). The nuclear membrane constitutes a second thin shell, surrounding a uniform sphere with fixed conductivity and permittivity. However, the dielectric properties of nucleated cells was not measured in this work as accurate modelling requires a much wider measurement window, extending to 300MHz. Furthermore, the parameter set becomes too large to obtain reliable fits to the data, particularly as the nuclear envelope is electrically leaky and the size of the nucleus is unknown. Nevertheless, the single cell analysis technique presented in this paper provides a new method that for the first time enables the dielectric properties of tens of thousands of single cells to be uniquely determined in an extremely short time window, thus enabling the identification of rare or outlier cells in a population which hitherto would not have been possible.

Acknowledgements

The authors would like to express their gratitude to Katie Chamberlain for fabrication of the impedance cytometer microchips.

Supporting Information

Supporting Information Available: The following files are available free of charge:
Supporting_information.docx Fig S1: Examples of single cell dielectric spectra of RBC ghosts from cells with an unusually low membrane capacitance. Fig S2: A comparison of the dielectric spectra of the RBC and ghost population average compared to the arithmetic mean of the single cell dielectric spectra. Details of the finite element method simulation.

Data access statement

All data supporting this study are openly available from the University of Southampton repository at https://doi.org/10.5258/SOTON/D1220

References

[1] Voldman J, *Electrical forces for microscale cell manipulation*, Annu Rev Biomed Eng. (2006), **8**, 425-54.

[2] Pethig R, *Review Article—Dielectrophoresis: Status of the theory, technology, and applications*, Biomicrofluid. (2010) **4**, 2: 022811; doi:10.1063/1.3456626

[3] Vahey MD and Voldman J, *An Equilibrium Method for Continuous-Flow Cell Sorting Using Dielectrophoresis*, Anal. Chem. (2008), **80** (9) 3135-3143.

[4] Vahey MD and Voldman J, *High-Throughput Cell and Particle Characterization Using Isodielectric Separation*, Anal. Chem. (2009) **81**, 2446–2455.

[5] Jaffe A and Voldman J, *Multi-frequency dielectrophoretic characterization of single cells*, Microsyst. Nanoeng. (2018) 4:23; doi:10.1038/s41378-018-0023-4

[6] Pethig R, Lee RS and Talary MS, *Cell Physiometry Tools Based on Dielectrophoresis*, JALA (2004), **9** (5) 324-330

[7] Xie X, Zhang Z, Ge X, Zhao X, Hao L, Cheng Z, Zhou W, Du Y, Wang L, Tian F, Xu X, *Particle Self-Aligning, Focusing, and Electric Impedance Microcytometer Device for Label-Free Single Cell Morphology Discrimination and Yeast Budding Analysis*, Anal. Chem. (2019), **91**, 21, 13398-13406

[8] Liu J, Qiang Y, Alvarez O and Du E, Electrical impedance microflow cytometry with oxygen control for detection of sickle cells, Sensors and Actuators B: Chemical (2018), **255**, 2392-2398

[9] Sun T, and Morgan H, *Single-cell microfluidic impedance cytometry: a review*, Microfluid. Nanofluid. (2010) **8**, 423-443

[10] Cheung KC, Berardino MD, Schade-Kampmann G, Hebeisen M, Pierzchalski A, Bocsi J, Mittag A, Tárnok A, *Microfluidic impedance-based flow cytometry*, Cytometry (2010) **77A**, 648-666.

[11] Chen J, Xue C, Zhao Y, Chen D, Wu MH,and Wang J, *Microfluidic Impedance Flow Cytometry Enabling High-Throughput Single-Cell Electrical Property Characterization*, Int J Mol Sci. (2015) **16,** 5, 9804–9830

[12] Morgan H, Sun T, Holmes D, Gawad S and Green NG, *Single cell dielectric spectroscopy*, J. Phys. D: Appl. Phys. (2007) **40** 61–70.

[13] Foster KR and Schwan HP, *Dielectric properties of tissues and biological materials: a critical review,* Crit Rev Biomed Eng. (1989), **17** (1), 25-104.

[14] Pauly, H and Schwan HP, *On the dielectric properties of a suspension of spherical particles covered by a shell*, Z Naturforsch (1959), **14b**, 125-131.

[15] Spencer D and Morgan H, *Positional dependence of particles in microfludic impedance cytometry*, Lab Chip (2011), **7** (11) 1234-1239.

[16] Spencer D, Caselli F, Bisegna P and Morgan H, *High accuracy particle analysis using sheathless microfluidic impedance cytometry,* Lab Chip (2016), **16** 2467-2473.

[17] Reale R, De Ninno A, Businaro Lm Bisegna P and Caselli F, *Electrical measurement of cross-sectional position of particles flowing through a microchannel*, Microfluid. Nanofluid. (2018), 22:41; doi: 10.1007/s10404-018-2055-3

[18] Spencer D and Morgan H, *Apparatus for electrically measuring individual particles flowing in a liquid*, Patent#. 10,267,720 B2, Application#: 14/392,104. PCT Pub . No . : WO2014/170625; Date of Patent: Apr 23, 2019.

[19] Sun T, Green NG, Gawad S and Morgan H, *Analytical electric field and sensitivity analysis for two microfluidic impedance cytometer designs*, IET Nanobiotechnol. (2007), **1,** 69– 79.

[20] Kim YR and Ornstein L, *Isovolumetric sphering of erythrocytes for more accurate and precise cell volume measurement by flow cytometry*, Cytometry (1983), **3** (6) 419-27.

[21] Migneault I, Dartiguenave C, Bertrand MJ, and Waldron KC, *Glutaraldehyde: behavior in aqueous solution, reaction with proteins, and application to enzyme crosslinking* BioTechniques (2004) **37** (5) 790-802.

[22] Beving H, Eriksson LE, Davey CL and Kell DB, *Dielectric properties of human blood and erythrocytes at radio frequencies (0.2-10 MHz); dependence on cell volume fraction and medium composition*, Eur Biophys J (1994), **23** 207-15.

[23] Asami K, Takahashi Y and Takashima S, *Dielectric properties of mouse lymphocytes and erythrocytes*. Biochim Biophys Acta (1989), **1010** 49-55.

[24] Gimsa J, Schnelle T, Zechel G and Glaser R, *Dielectric spectroscopy of human erythrocytes: investigations under the influence of nystatin,* Biophys J (1994), 66 1244–1253.

[25] Lisin R, Ginzburg BZ, Schlesinger M and Feldman Y, *Time domain dielectric spectroscopy study of human cells. I. Erythrocytes and ghosts*. Biochimica et Biophysics Acta (1996), **1280** 34-40.

[26] Bordi F, Cametti C and Gili T, *Dielectric spectroscopy of erythrocyte cell suspensions. A comparison between Looyenga and Maxwell–Wagner–Hanai effective medium theory formulations,* J Non-Cryst Solids (2002), **305** 278-284.

[27] Bao JZ, Davis CC and Schmukler RE, *Frequency domain impedance measurements of erythrocytes. Constant phase angle impedance characteristics and a phase transition*, Biophys J (1992), **61** 1427–1434.

[28] Spencer D, Hollis V and Morgan H, *Microfluidic impedance cytometry of tumour cells in blood*, Biomicrofluidics (2014), **8** (6): 064124; doi: 10.1063/1.4904405

[29] Gagnon Z, Gordon J, Sengupta S and Chang HC, *Bovine red blood cell starvation age discrimination through a glutaraldehyde-amplified dielectrophoretic approach with buffer selection and membrane cross-linking*. Electrophoresis (2008) **29** (11) 2272-2279

[30] Cheung K, Gawad S and Renaud P, *Impedance Spectroscopy Flow Cytometry: On-Chip Label-Free Cell Differentiation*, Cytometry Part A (2005), 65A:124–132.

[31] Bone S, Ginzburg BZ, Morgan H, Wilson G and Zaba B, Time-domain dielectric spectroscopy applied to cell suspensions, Phys. Med. Biol. (1993), **38** 511-520.

[32] Honrado C, Ciuffreda L, Spencer D, Ranford-Cartwright L and Morgan H, *Dielectric characterization of Plasmodium falciparum infected red blood cells using microfluidic impedance cytometry*, J R Soc Interface (2018), **15:**20180416; doi: 10.1098/rsif.2018.0416

[33] Shaker M, Colella L, Caselli F, Bisegna P and Renaud P, *An impedance-based flow microcytometer for single cell morphology discrimination*, Lab Chip (2014), **14** 2548-2555.

For TOC only

Graphical abstract

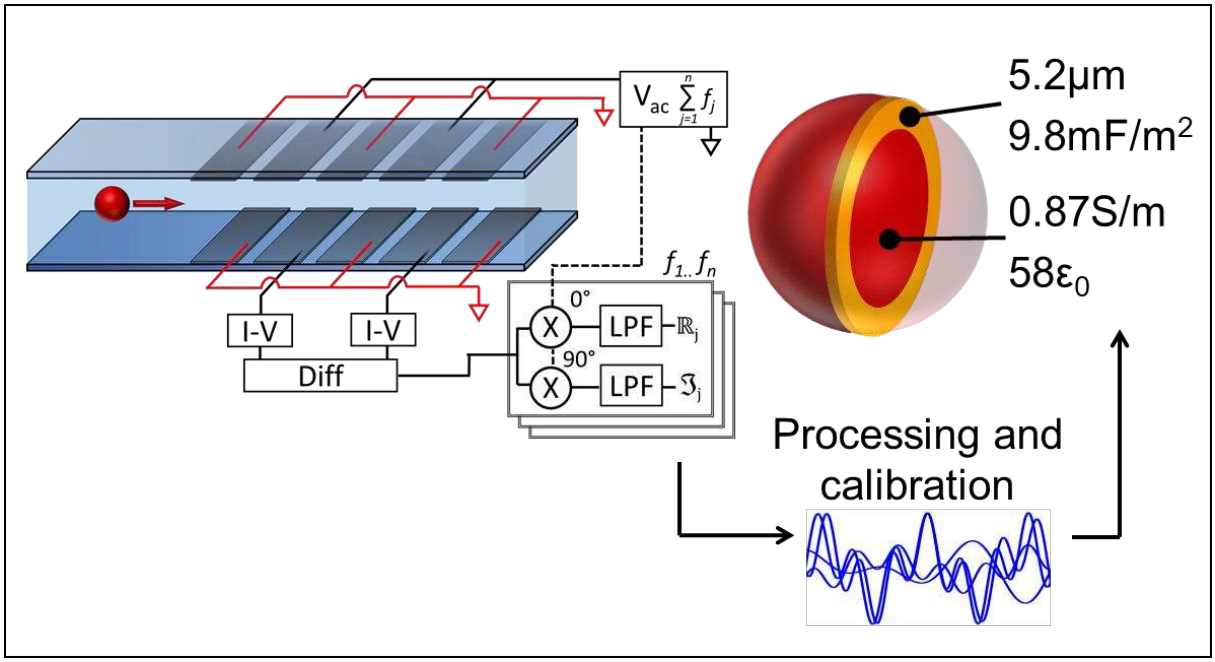

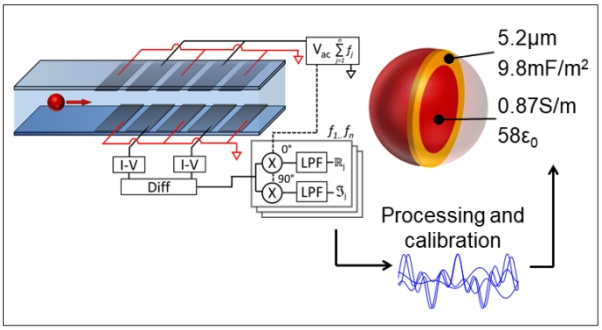

338x190mm (96 x 96 DPI)

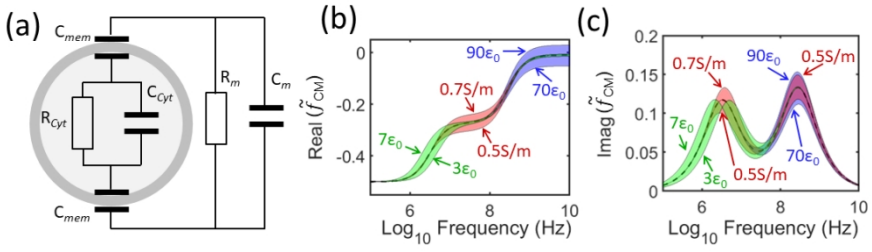

Figure 1

338x190mm (96 x 96 DPI)

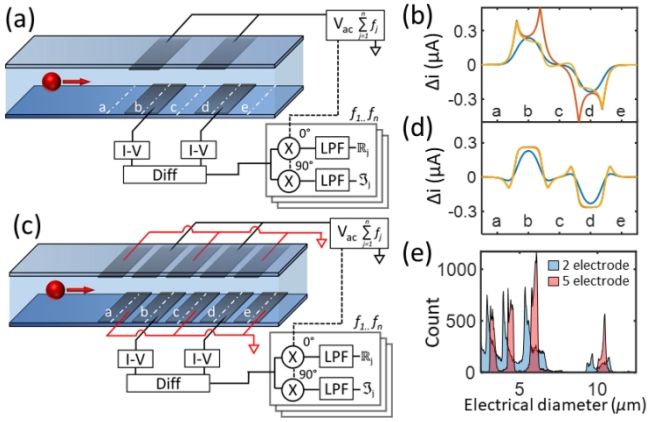

Figure 2

338x190mm (96 x 96 DPI)

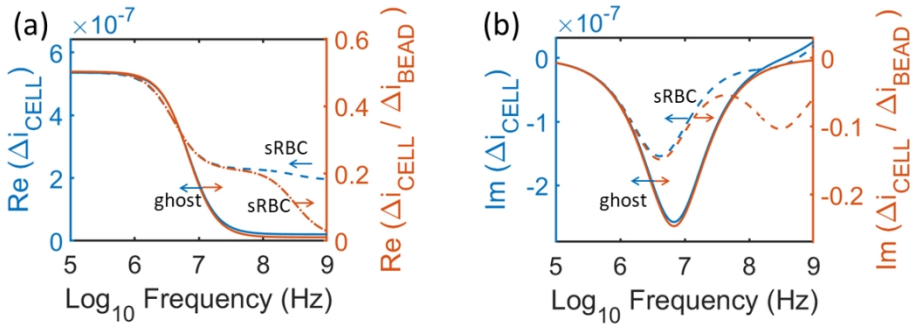

Figure 3

338x190mm (96 x 96 DPI)

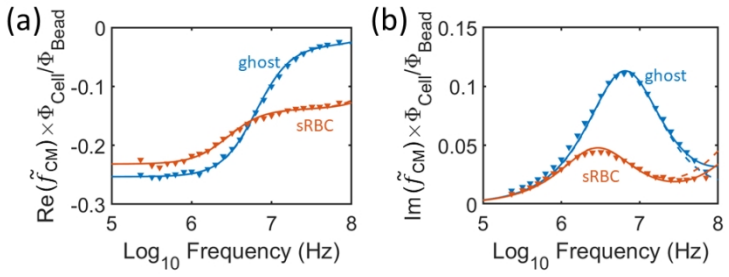

Figure 4

338x190mm (96 x 96 DPI)

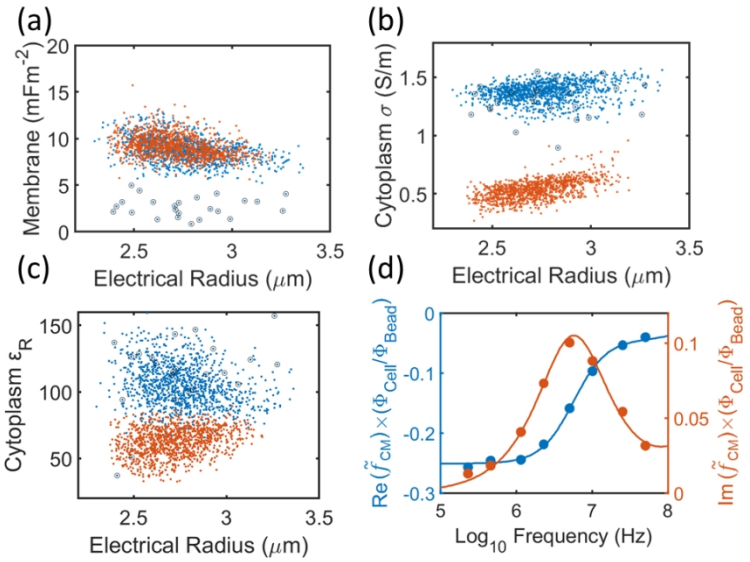

Figure 5

338x190mm (96 x 96 DPI)

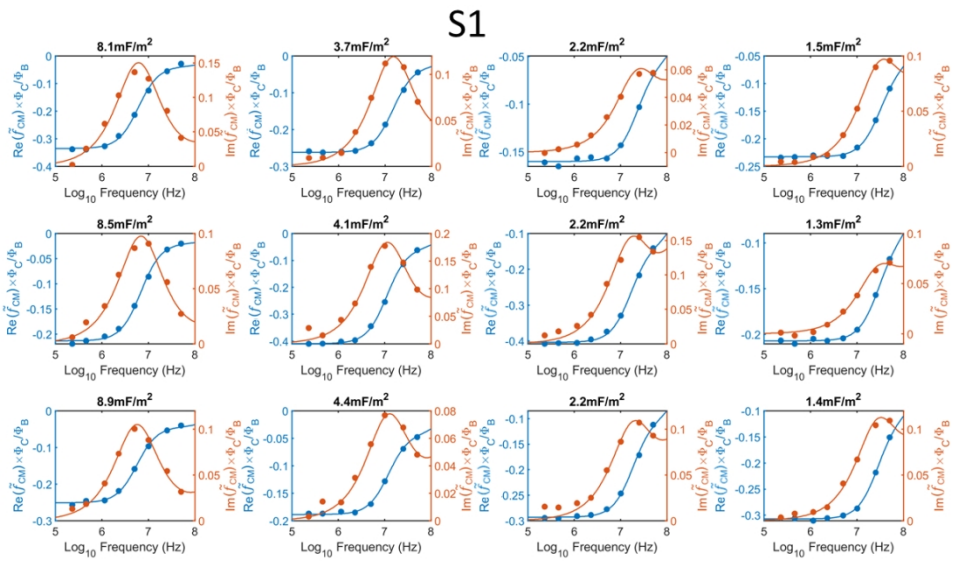

Figure S1

338x190mm (96 x 96 DPI)

S2

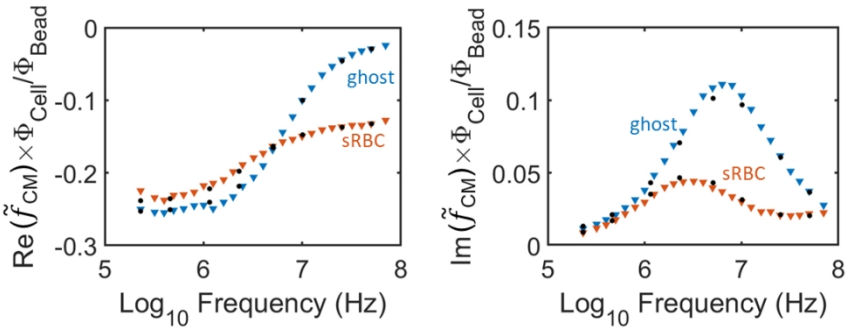

Figure S2

338x190mm (96 x 96 DPI)